FERROELECTRIC AND DIELECTRIC PROPERTIES OF NICKEL DOPED BaTiO$_3$ THIN FILMS DEVELOPED BY SOL-GEL SPIN-COATING PROCESS

M. Y. SHAHID[a*], M. ASGHAR[a], F. MALIK[a], M. F. WARSI[b]

[a]*Department of Physics, The Islamia University of Bahawalpur, Bahawalpur-63100, Pakistan*

[b]*Department of Chemistry, Baghdad-ul-Jadeed Campus, The Islamia University of Bahawalpur, Bahawalpur-63100, Pakistan*

Polycrystalline thin films of BaTiO$_3$ + xNi (BTN), here x = 0.0, 0.025, 0.05, 0.1, 0.2, 0.3 and 0.4 have been systematically obtained by sol–gel spin-coating technique. Ti-foils have been used as a substrate. Various characterization techniques have been used to study the structure, ferroelectric and dielectric properties of the BTN films such as X-ray diffraction (XRD), scanning electron microscopy (SEM), electron probe micro analyzer (EPMA) and etc. Ni-doped BaTiO$_3$ thin films show many interesting results, such as shifting in the diffraction peaks, enhancement in ferroelectric and dielectric properties. The XRD pattern of BTN films show a slight shift in diffraction peaks to the higher 2-theeta Bragg's angle with the addition of Ni-content. Lattice constants are found using XRD plots. With the addition of Ni-dopant in BaTiO$_3$, no phase change in the crystal structure has been observed. The SEM micrographs of BTN films display the crack free as well as uniform nature of the grown films. It is explored that the control of the process, specifically in the early stage of drying process, is essential and imperative for the synthesis of crack-free Ni-doped BaTiO$_3$ thin films. The EPMA certifies the elemental composition of the grown samples. The electrochemical measurements of BTN films present the change in the current density (J) with the applied voltage (V). The polarization-voltage (P-V) analysis of these thin films shows the enhancement in the ferroelectric properties with Ni-content. Moreover dielectric constant vs frequency (ε_r - f) measurements reveal that dielectric constant increases with Ni-dopant concentration. Among these BTN samples, the compositions BaTiO$_3$+0.4Ni films have the highest value of the dielectric constant i.e. 2.39×10^{-35} measured at 10MHz frequency at room temperature. The ferroelectric and dielectric properties of the sol-gel synthesized BTN thin films are inclined by the Ni-dopant. Doping has a vital effect on both ferroelectric as well as dielectric properties of a material that is highly appreciated in making high frequency devices.

1. Introduction

Barium titanate (BaTiO$_3$) is a well-known ferroelectric as well as dielectric material with perovskite structure having a wide range of applications such as piezoelectric, dielectric, micro-electro mechanical systems (MEMS), multilayer ceramic capacitors (MLCs)[1], piezoelectric transducers, microwave devices, different type of storage information devices, infrared sensors[2-4]. Recently, as-grown and doped BaTiO$_3$ thin films have attracted much more attention because of their intense use as PTC thermistors, pyro-electric detectors, multilayer hybrid capacitors and electro-optic devices[5]. The ferroelectric and dielectric properties of BaTiO$_3$ can be well managed by doping with a variety of dopant elements [6-9]. The potential applications of nickel-doped BaTiO$_3$ bulk materials are still discovered over a considerable range of compositions. Few reports are available on this subject where the micro-structural variations in Ni-doped barium titanate[10],

---

* Corresponding author: yarmuhammadshahid@gmail.com

dielectric properties of nickel-doped $BaTiO_3$ nanoparticles [10], exaggerated grain growth in Ni-doped $BaTiO_3$, dielectric characteristics of $BaTiO_3$ doped with Nb and Ni [11], electrical transport behavior of $BaTiO_3$ co-doped with Ni and Mn at high temperature[12], phase stability and valence change of Ni-doped $BaTiO_3$ annealed in H_2 and O_2 have been discussed [13]. The ionic radii of Ni^{2+} ($r_6^{2+} = 0.69$Å) is less than both ions Ba^{2+} ($r_6^{2+} = 1.35$Å) and Ti^{4+} ($r_6^{4+} = 0.61$Å) and therefore it can occupy both Ba^{2+} and Ti^{2+} ions sites. According to our literature review no systematic study of ferroelectric and dielectric properties of Ni-doped $BaTiO_3$ thin films has been stated. The growth and characterization of Ni-doped $BaTiO_3$ thin films via spin-coating sol-gel process is presented first time. The fabrication of many novel devices is based on Ni-doped $BaTiO_3$ thin films that include thin film capacitors, optoelectronic devices, phase shifters, photovoltaic devices and humidity sensors[14]. This is the motivation of our work. There are many film deposition techniques that have been practiced to prepare $BaTiO_3$ films including sputtering[15], metal organic chemical vapor deposition (MOCVD)[16-18], laser ablation and sol-gel process[19]. The sol-gel process has certain advantages over other depositing methods such as cost, purity, homogeneity and process control[20, 21]. The ferroelectric and dielectric properties of $BaTiO_3+$ xNi greatly depend on the Ni-concentration.

In this work the structure, dielectric and ferroelectric properties of Ni-doped $BaTiO_3$ have been studied systematically and the effect of Ni-doping on the properties of $BaTiO_3$ thin films has been investigated.

2. Experimental details

Thin films of nickel-doped barium titanate with the compositional formula $BaTiO_3+$xNi (BTN), here x = 0.0, 0.025, 0.05, 0.1, 0.2, 0.3, and 0.4, were obtained by sol-gel synthesis method. The precursor materials used initially were barium acetate (Ba $(C_2H_3O_2)_2$) (Aldrich, St. Louis, MO – 24,367, 99%), titanium (iv) n-butoxide ($C_{16}H_{36}O_4Ti$) (Aldrich – 205,273, 97%), and Nickel acetate ($Ni(CH_3CO_2)_2·2H_2O$) (Aldrich – 227,676, 99%). The precursor materials were weighed according to the stoichiometric quantities and mixed thoroughly in aqueous phases for homogenization of the compositions. At first, the measured amounts of nickel acetate and barium acetate were mixed in heated glacial acetic acid. The resulting solution was stirred constantly until all the particles were dissolved. Secondly the suitable amount of titanium (iv) *n*-butoxide was dissolved in 2-methoxyethanol and added to the already prepared solution under the continuous stirring. As a stabilizer ethylene glycol was added to this solution in 1:3 proportions to the glacial acetic acid. The precursor solutions of $BaTiO_3+$ xNi with concentration x= 0.0, 0.025, 0.05, 0.1, 0.2, 0. 3 and 0.4 were obtained. The molarity of all prepared solutions was maintained at 0.4 M for spin-coating on titanium (Ti) substrates. Before spin coating, titanium substrates were cleaned with acetone, isopropyl alcohol and deionized water at 80 ^{o}C for 10 minutes in each and then dried in air. A thin film comprises three layers of coating and each layer was subjected to a controlled heat treatment cycle in a rapid thermal processor. Every spin coated layer was dried at 100 ^{o}C for 10 min in a muffle furnace, in this way a thin film was prepared by three layers. Finally, the whole film was annealed at 750 ^{o}C for 2-h in air atmosphere. Table 1 presents the detailed of the amounts of compounds used for the preparation of samples of various compositions of $BaTiO_3+$ xNi.

The crystal structure and phase formation of BTN thin films were studied using a Philips PW3710 X-ray diffractometer (XRD) in a glancing angle mode using Cu-Kα radiation source of wave length λ = 1.54056Å with a Ni-filter. The XRD plots of films were taken in the range of 20–60° of diffraction angles (2θ). The microstructural characterizations were done by using a scanning electron microscope (SEM). Electron probe micro analyzer (EPMA) was used to check the chemical compositions at the various spots of Ni-doped $BaTiO_3$ thin films. For electrical measurements, a gold film of 200 nm thickness was deposited on BTN films by thermal evaporation technique to form a metal–ferroelectric–metal (MFM) configuration. The dielectric properties measurements of Ni-doped $BaTiO_3$ thin films were taken using a Hewlett-Packard 4275A multi-frequency LCR meter with 16047A test fixture. Polarization–applied voltage (P-V) hysteresis loops were taken using a modified Sawyer Tower circuit. AC electrochemical

measurements were done with a Solartron 1260 frequency analyzer (FRA) in series with a Princeton Applied Research (PAR) 263A potentiostat. The flow chart in Fig. 1 presents the summary of the steps used to deposit BTN thin films.

Table 1: Different amounts of compounds for different compositions of BaTiO₃+xNi

| Sr. No.	Ni-composition	X=0.0M	X=0.025M	X=0.05M	X=0.1M	X=0.2M	X=0.3M	X=0.4M
1	Barium acetate (Ba(C$_2$H$_3$O$_2$)$_2$)	1.53g	1.53g	1.53g	1.53g	1.53g	1.53g	1.53g
2	Titanium (iv) n-butoxide (Ti(C$_{16}$H$_{36}$O$_4$))	2.11ml	2.11ml	2.11ml	2.11ml	2.11ml	2.11ml	2.11ml
3	Nickel (ii) acetate (Ni(CH$_3$COO)$_2$·2H$_2$O)	0.0g	0.066g	0.133g	0.266g	0.530g	0.796g	1.061g
4	Glacial acetic acid	15ml	15ml	15ml	15ml	15ml	15ml	15ml
5	2-methoxyethanol	15ml	15ml	15ml	15ml	15ml	15ml	15ml
6	ethylene glycol	5ml	5ml	5ml	5ml	5ml	5ml	5ml
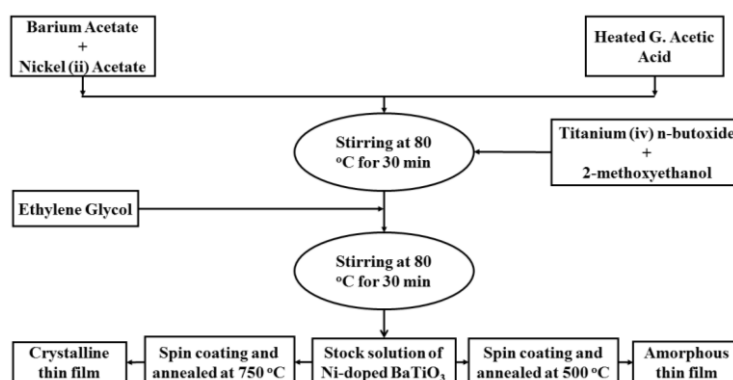
Fig. 1: Flow chart illustrating the major steps involved in the synthesis of Ni-doped BaTiO₃

3. Results and discussions

3.1 X-ray diffraction (XRD)

The XRD patterns for the BTN thin films grown by sol-gel process on Ti-substrate are shown in Fig. 2. Sharp peaks in all XRD graphs were detectable and hence it was verified that all the prepared samples were well crystallized and phase pure. Diffraction peaks occurred at slightly larger angles when the samples were doped with Ni ion. The XRD results showed that the prepared samples have tetragonal phase. The calculated lattice parameters and hkl of selected peaks at diffraction angle (2θ) for tetragonal structure were given in the Table 2.

It is obvious from the data that Ni-doping results a shortening of the a-axis and lengthening of the c-axis to produce a more tetragonal structure with a slight variation in cell volume. It is also observed that Ni-concentration decreases the lattice constant and crystallite size. But the samples do not display any phase relating to NiO compound. Therefore it appears that Ni^{2+} ions are totally soluble in BaTiO$_3$ lattice with the possibility of the Ni^{2+} (0.69 Å) ions replacing both Ti^{4+} (0.61 Å) and Ba^{2+} (1.36 Å) sites due to its small ionic radius. The addition of Ni-doping concentration, no phase change of the BTN thin films was observed but it was observed that there was a slight shift in the XRD peaks to the higher diffraction angle displaying lower values of lattice constant. Therefore, it can be resulted that the incorporation of Ni-content to BTN cannot

alter the crystal structure of the BTN. The slight shift in the diffraction peaks could be explained on the basis of shrinking the crystal lattice due to the incorporation of the Ni-dopant that may be due to the replacement of large ionic radii of Ba^{2+} (1.36 Å) ion with smaller ionic radii Ni^{2+} (0.69 Å)[22, 23].

Table 2: Lattice constant for different compositions of $BaTiO_3+xNi$

| Composition	X=0.00	X=0.025	X=0.05	X=0.1	X=0.2	X=0.3	X=0.4
hkl	2θ	2θ	2θ	2θ	2θ	2θ	2θ
103	27.408	27.657	27.657	27.408	27.813	27.371	27.896
110	31.481	31.647	31.730	31.398	31.803	31.730	31.969
105	35.959	36.291	36.291	35.949	36.447	36.291	36.447
111	37.839	37.995	38.078	37.839	38.244	38.041	38.410
203	39.958	40.115	40.115	39.958	40.281	40.281	40.483
210	52.499	52.665	52.739	52.665	52.904	52.739	52.987
213	54.213	54.572	54.535	54.287	54.701	54.535	54.784
Lattice Constant a (Å)	4.072242	4.056703	4.053574	4.067894	4.04112	4.049644	4.028307
Lattice Constant c (Å)	17.13587	16.90563	16.93487	17.16564	16.83426	16.9032	16.84618
c (Å) / a (Å)	3.6286	4.1673	4.1778	4.2198	4.1657	4.1740	4.1820
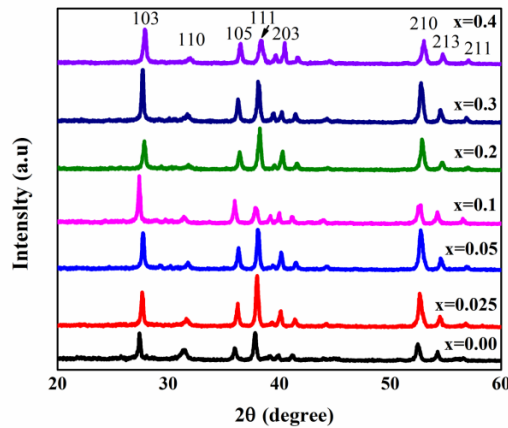
Fig. 2: XRD patterns of the $BaTiO_3$ + xNi thin films grown by sol-gel process (where x = 0.0, 0.025, 0.05, 0.1, 0.2, 0.3, and 0.4) annealed at 750 ^{o}C.

3.2 Scanning electron microscope (SEM)

The SEM micrographs of $BaTiO_3+Ni_x$ thin films for x = 0.0, 0.025, 0.050, 0.1, 0.2, 0.3, and 0.4 are shown in Fig. 3. The SEM images indicate well crystallized and crack free nature thin films. As it can be observed from Fig. 3, the surface cracks of $BaTiO_3$ + xNi thin films are dependent on Ni-concentration and the film cracks decrease with the increase in Ni-content. The specimen with higher concentration in our experiment has almost crack free surface. Thin film made from an un-doped $BaTiO_3$ precursor solution have a surface with large cracks shown in Fig.3 (x=0.0). On the other hand, BTN film made from a $BaTiO_3$ precursor solution with maximum Ni-dopant concentration ($BaTiO_3$ + xNi for x=0.4) in these samples, have a surface with no cracks (uniform) presented in Fig.3 (x=0.4). A comparable pattern has been presented for MOD grown BST films with reduced grain sizes[24]. This indicates that thin film surface morphology depends on Ni-concentration.
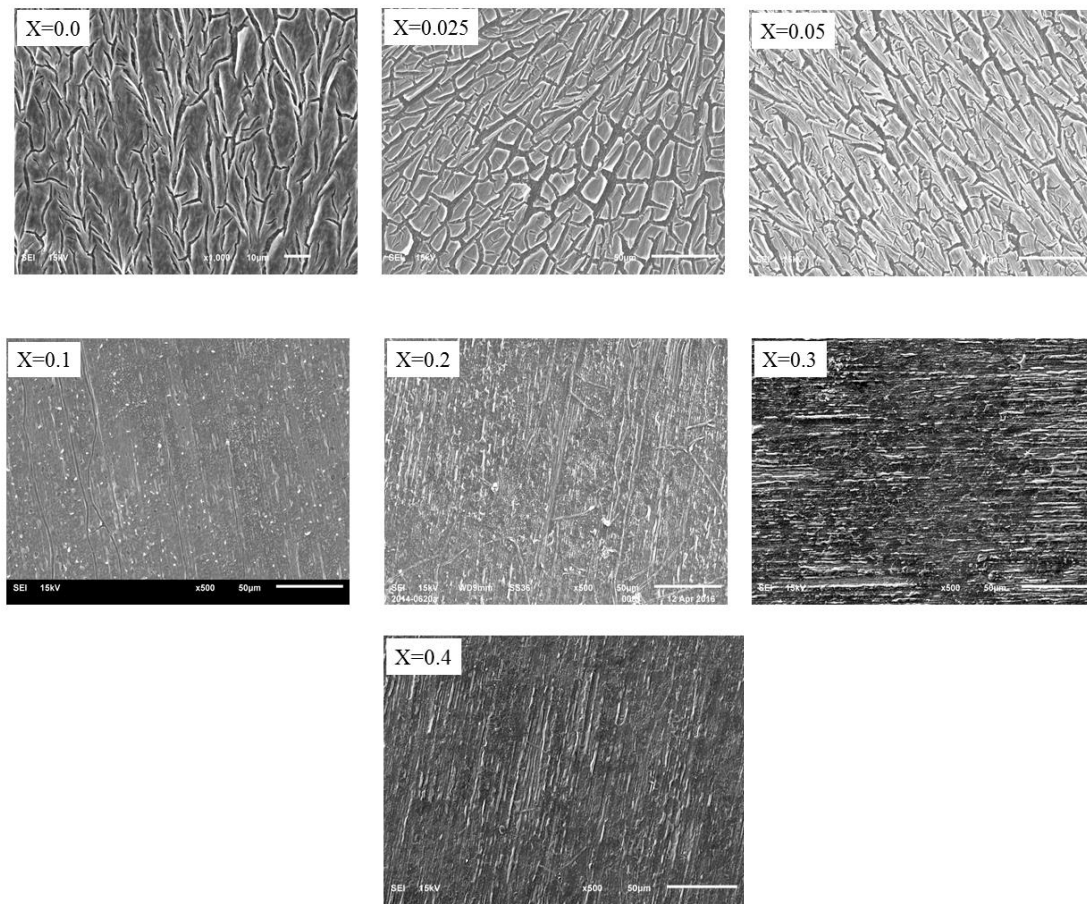
Fig. 3: SEM micrographs of BaTiO₃ + xNi thin films for the different concentration of Ni

3.3 Electron probe micro analyzer (EPMA)

Table 3 presents the results of the elemental analysis of un-doped and Ni-doped $BaTiO_3$ thin films grown by sol-gel spin-coating process. This method for elemental composition of the samples has been used because this method has certain advantages over other elemental composition techniques especially when it comes to multicomponent metal oxides. EPMA data shown in Table 3 confirms the elemental composition of the prepared samples and the samples were found to be of the same composition that we have prepared.

Table 3: (a) EPMA data of the surface analysis of the composition $BaTiO_3$ + xNi
(Where x = 0, 0.0250 and 0.050) thin films in molar percent.

Composition	Ba (%)	Ti (%)	Ni (%)	Cl (%)
$BaTiO_3$	49.1696	49.1699	-	1.6605
$BaTiO_3$+0.025Ni	46.9637	46.9637	3.4891	2.5835
$BaTiO_3$+0.05Ni	45.3149	45.3124	6.9229	2.4499

(b) EPMA data of the surface analysis of the composition BaTiO₃ + xNi
(Where x = 0.1, 0.2, 0.3, and 0.4) thin films in atomic percent.

Composition	Ba (%)	Ti (%)	Ni (%)	Cl (%)	O (%)
BaTiO$_3$+0.1Ni	18.085	18.085	4.389	1.593	57.848
BaTiO$_3$+0.2Ni	16.655	16.655	7.037	5.302	54.351
BaTiO$_3$+0.3Ni	15.412	15.412	10.314	4.622	54.239
BaTiO$_3$+0.4Ni	14.588	14.588	12.278	5.008	53.538

3.4 Ferroelectric properties measurements

For electrical measurements of the prepared samples, a gold film of thickness 200 nm and surface area (1.5×1.5) cm^2 was deposited on the samples by thermal evaporating technique to make a configuration such as metal-ferroelectric-metal (MFM). Fig. 4 presents the room temperature P-V hysteresis graphs of the composition BaTiO$_3$ + xNi (where x= 0.025, 0.05, 0.1, 0.2, 0.3 and 0.4) thin films. From these plots it is evident that the value of remnant polarization and the shape of the hysteresis loops mainly depend on Ni-doping concentration[25]. The P-V loops are swells out as the Ni-dopant concentration is increased. From the Fig. 4 it is also clear that remnant polarization values of the thin films increase with increasing Ni-concentration. The remnant polarization values vs various Ni-concentrations taken at applied voltage 0.72V are shown in Table 4.

Table 4: Remnant Polarization vs different Ni-concentration data of BaTiO₃ + xNi thin films

Composition	Polarization (uC/cm^2)	Driven voltage(V)
BaTiO$_3$	4.2239E-6	7.5316E-1
BaTiO$_3$+0.025Ni	5.0863E-6	7.6050E-1
BaTiO$_3$+0.05Ni	6.8860E-6	7.1410E-1
BaTiO$_3$+0.1Ni	7.6613E-6	7.7515E-1
BaTiO$_3$+0.2Ni	1.5767E-5	7.2386E-1
BaTiO$_3$+0.3Ni	1.6530E-5	7.8480E-1
BaTiO$_3$+0.4Ni	1.7756E-5	7.0677E-1

The plot between polarization and various Ni-concentrations displayed in Fig. 5. From the Fig. 5 it is clear that polarization increases with Ni-dopant concentration. A well-defined loop was obtained from BaTiO$_3$ + 0.4Ni due to its larger surface homogeneity. The ferroelectric properties of BaTiO$_3$ + xNi thin films strongly depend on the Ni-dopant concentration and homogeneity of the surface[26]. The film made from a BaTiO$_3$ precursor solution with no Ni-content (BaTiO$_3$ + xNi for x=0.0) in these samples showed a slim hysteresis P-V loop shown by Fig. 4(x=0.0). While the film made from a BaTiO$_3$ precursor solution with a maximum Ni-concentration (BaTiO$_3$ + xNi for x=0.4) in these samples showed a broad hysteresis P-V loop shown by Fig. 4(x=0.4). The ferroelectric properties of BTN thin films greatly depend on the Ni-concentration.
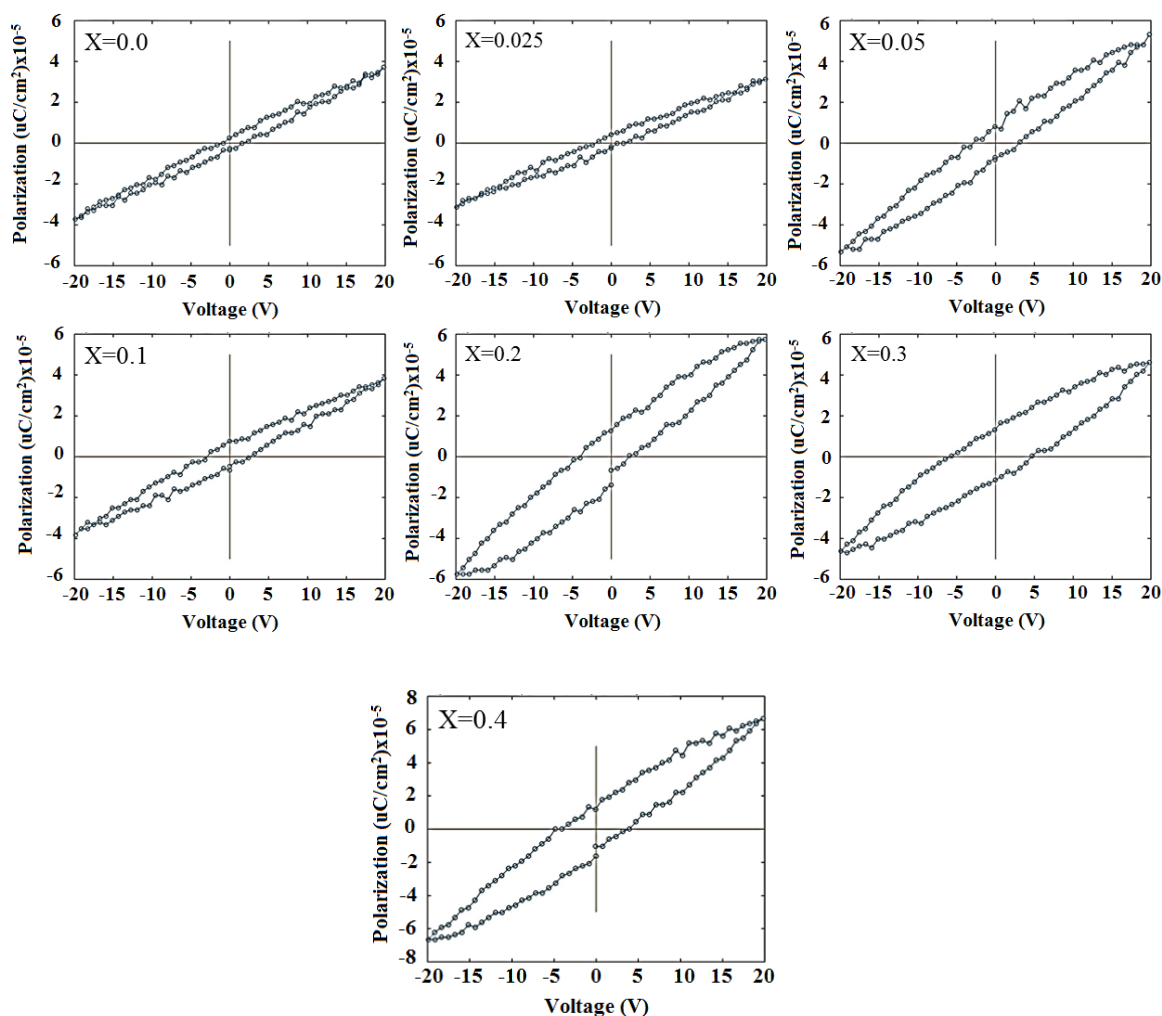
Fig. 4: Polarization-applied voltage (P-V) hysteresis measurements
of BaTiO₃ + xNi thin films prepared by sol-gel method

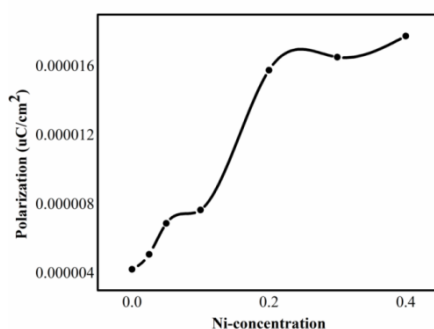*Fig. 5: Polarization vs Ni-concentration of BaTiO₃ + xNi thin films prepared by sol-gel method*

3.5 Electrochemical measurements

Current density-working potential (J-V) of $BaTiO_3$ + xNi thin films of different Ni-concentration are shown in Fig. 6. Increasing the voltage window much beyond 500V to -2000 mV vs standard hydrogen electrode resulted in the evolution of hydrogen or oxygen as discussed below. The broadening of the peaks increases with Ni-concentration in $BaTiO_3$ + xNi thin films.

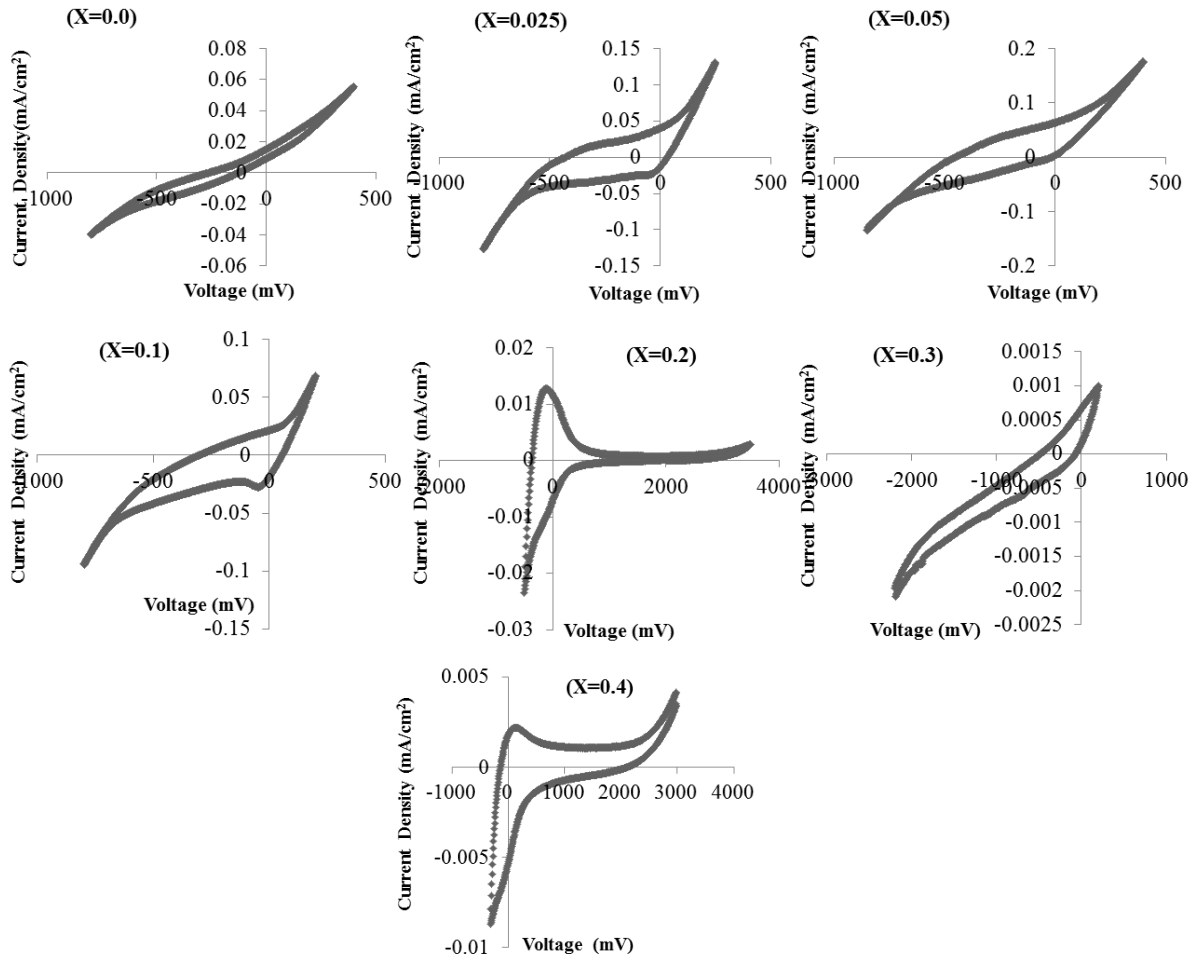*Fig. 6: Typical Cyclic volta-mamograms of un-doped and nickel-doped $BaTiO_3 + xNi$ thin films in 0.05M H_2SO_4. 200mV/s scan rate*

3.6 Dielectric properties measurements

The dielectric constant, dielectric loss and capacitance of a material are the important parameters that are used in the selection a material for suitable applications. The dielectric constant (ε_r) of a given material is determined by using the equation given below:

$$\varepsilon_r = \frac{Cd}{\varepsilon_o A}$$

Where 'C' denotes the capacitance 'd' represents the thickness of the dielectric material (film), the permittivity of free space is denoted by 'ε_o' and 'A' show the surface area of the dielectric material (film). The behavior of dielectric constant (ε_r) as a function of frequency for the various compositions of the BTN thin films obtained at room temperature is shown in Fig. 7. The thin film having composition $BaTiO_3 + xNi$ (maximum Ni-content) possesses the maximum dielectric properties in these samples. While the film made from a $BaTiO_3$ precursor solution having no Ni-content ($BaTiO_3 + xNi$ for x=0.0) in these samples possesses the minimum dielectric constant. Table 5 shows the dielectric constant measured at different frequencies for all the prepared samples. It is observed that ε_r increases with increasing Ni-dopant concentration. A similar behavior has been presented for sol-gel derived BST thin films on Si-substrate[27].

Table 5: Dielectric constant vs frequency data of un-doped and nickel-doped BaTiO$_3$ + xNi thin films.

Frequency (MHz)	X = 0.0	X = 0.025	X = 0.05	X = 0.1	X = 0.2	X = 0.3	X = 0.4
0.01	0.00256	0.001867	0.001825	0.008984	0.002642	0.005821	0.002861
0.02	0.00229	0.001789	0.001795	0.007271	0.002476	0.005073	0.00284
0.10	0.001867	0.001634	0.001709	0.003359	0.002145	0.003701	0.002696
0.40	0.001645	0.001551	0.001659	0.002396	0.001951	0.002941	0.002578
2.00	0.001484	0.001479	0.0016	0.001882	0.0018	0.002446	0.002522
10.00	0.001337	0.001379	0.001487	0.001556	0.001655	0.00206	0.002393

Dielectric constant as a function of different composition of the samples is plotted and shown in the Fig. 8. It is obvious from this plot that the variation of dielectric constant with composition of the samples is nearly linear. The dielectric constant decreases with increasing the operating frequency within the range of 10 KHz to 10 MHz and after 1MHz, the dielectric constants was decreased to some extent or nearly remain constant showing that the grown BTN films have stable dielectric properties in the high frequency range.
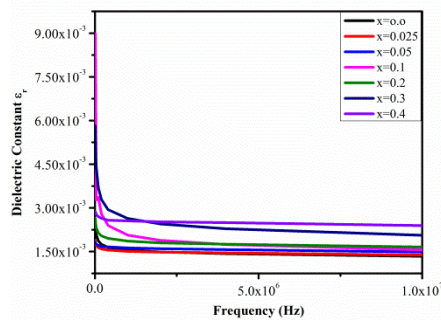

Fig. 7: Dielectric constant as a function of frequency at room temperature of BaTiO$_3$ + xNi thin films

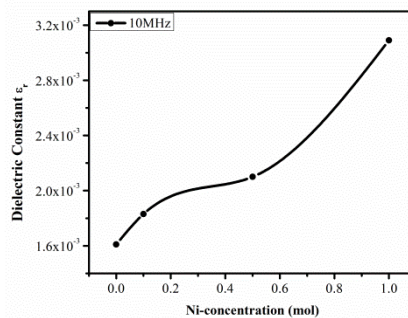*Fig. 8: Dielectric constant vs Ni-concentration (mol) of the samples*

4. Conclusion

The thin films with the compositions $BaTiO_3$ + xNi where x = 0, 0.025, 0.05, 0.1, 0.2, 0.3 and 0.4 were synthesized on well cleaned Ti-substrate by the easiest and low cost sol-gel spin coating method for the first time. XRD results exposed that the films are polycrystalline nature and grown film has a tetragonal crystal structure. With Ni-doping in BaTiO3 films, no phase change in the structure was observed, however the decrease in lattice constant and crystallite size was observed with Ni-doping concentration. The XRD peaks shift to the higher 2-theta angle with the addition of Ni-concentration. The SEM micrographs displayed the homogeneous surface morphology and the EPMA results verified the composition of the grown samples. Both the dielectric constant and polarization increases with the Ni-incorporation. On the basis of good characteristics and properties, such materials have vital applications in the manufacturing of advance technological devices.

Acknowledgements

References

[1] K.B. Kim, T.S. Yun, R.Y. Kim, H.S. Kim, H.G. Kim, J.C. Lee, Microwave and optical technology letters **45,** 15 (2005).

[2] W. Maison, R. Kleeberg, R.B. Heimann, S. Phanichphant, Journal of the European Ceramic Society **23,** 127 (2003).

[3] J.S. Obhi, A. Patel, Integrated Ferroelectrics **5,** 155 (1994).

[4] J. Scott, D. Galt, J.C. Price, J.A. Beall, R.H. Ono, C.A. Paz de Araujo, L. McMillan, Integrated Ferroelectrics **6,** 189 (1995).

[5] Z. Fang, C. Shen, T. Qiu, Electronic Components and Materials **10,** 022 (2010).

[6] G.M. Keith, M.J. Rampling, K. Sarma, N.M. Alford, D.C. Sinclair, Journal of the European Ceramic Society **24,** 1721 (2004).

[7] P. Goel, K.L. Yadav, A.R. James, Journal of Physics D: Applied Physics **37,** 3174 (2004).

[8] P. Goel, K.L. Yadav, Journal of materials science **42,** 3928 (2007).

[9] M.A. Mohiddon, K.L. Yadav, Journal of sol-gel science and technology **49**, 88 (2009).

[10] A. Jana, T.K. Kundu, Materials Letters **61**, 1544 (2007).

[11] S. Wang, S. Zhang, X. Zhou, B. Li, Z. Chen, Materials Letters **60**, 909 (2006).

[12] E. Duverger, B. Jannot, M. Maglione, M. Jannin, Solid state ionics **73,** 139 (1994).

[13] R.D. Levi, Y. Tsur, Advanced Materials **17**, 1606 (2005).

[14] S. Majumder, M. Jain, A. Martinez, R. Katiyar, F. Van Keuls, F. Miranda, Journal of Applied Physics **90,** 896 (2001).

[15] W.-J. Lee, I.-K. Park, G.-E. Jang, H.-G. Kim, Japanese journal of applied physics **34**, 196 (1995).

[16] T. Kim, Y. Yoon, S. Yom, C. Kim, Applied surface science **90**, 75 (1995).

[17] Y. Yoon, W. Kang, H. Shin, S. Yom, T. Kim, J.Y. Lee, D. Choi, S.S. Baek, Journal of applied physics **73**, 1547 (1993).

[18] B. Kwak, K. Zhang, E. Boyd, A. Erbil, B. Wilkens, Journal of applied physics **69**, 767 (1991).

[19] C. Lemoine, B. Gilbert, B. Michaux, J.-P. Pirard, A. Lecloux, Journal of non-crystalline solids **175,** 1 (1994).

[20] M. Burgos, M. Langlet, Thin Solid Films **349**, 19 (1999).

[21] M. Kamalasanan, N.D. Kumar, S. Chandra, Journal of applied physics **74,** 5679 (1993).

[22] V. Somani, S.J. Kalita, Journal of electroceramics **18**, 57 (2007).

[23] R.W. Kelsall, I.W. Hamley, M. Geoghegan, Wiley Online Library (2005).

[24] M.S. Mohammed, R. Naik, J.V. Mantese, N.W. Schubring, A.L. Micheli, A.B. Catalan, Journal of materials research **11,** 2588 (1996).

[25] Z. Ren, G. Xu, X. Wei, Y. Liu, X. Hou, P. Du, W. Weng, G. Shen, G. Han, Applied Physics Letters **91,** 063106 (2007).

[26] B. Santara, B. Pal, P.K. Giri, Journal of applied physics **110,** 114322 (2011).

[27] S. Adikary, H. Chan, Thin Solid Films **424,** 70 (2003).